ANNALS OF GEOPHYSICS, 64, 6, GM662, 2021; doi:10.4401/ag-8699
OPEN ACCESS

Paleomagnetic results from Western Anatolia: evidence of microblock rotations after emplacement of the lower Miocene Yuntdağ volcanic rocks

Mualla Cengiz[1], Savaş Karabulut[2], Ferhat Özçep[1], Burak Semih Çabuk[1], Friedrich Heller[3]

(1) İstanbul University-Cerrahpaşa, Faculty of Engineering, Department of Geophysical Engineering, İstanbul, Turkey
(2) Department of Civil Engineering, Gebze Technical University, Kocaeli, Turkey
(3) Institute of Geophysics, Department of Earth Sciences, ETH Zurich, Zurich, Switzerland

Article history: received June 15, 2021; accepted October 21, 2021

Abstract

The eastern Aegean region has undergone north dipping subduction in the Oligocene, followed by continental collision in the early Miocene and then Miocene-Pliocene extension, which was associated with widespread Miocene volcanism. The aim of this study is to assess evidence of crustal block rotations due to stress variations in the Dikili (İzmir) province, Western Anatolia, based on paleomagnetic data obtained from 35 independent sites in addition to data from 19 sites reported in earlier studies. The lower Miocene Yuntdağ volcanic rocks were erupted in three different structural blocks, the Bergama, Zeytindağ and Dikili blocks. Clockwise rotation is found in the Dikili and Zeytindağ blocks that varies from R (± ΔR) = 12.5° (± 7.4°) in the west to R (± ΔR) = 35.6° ± (13.2°) in the east of the Bakırçay graben, respectively. In contrast, a counterclockwise rotation of R (± ΔR) = -38.1° (± 6.4°) is estimated for the Bergama block, to the north of the Dikili and Zeytindağ blocks. A scissor-like basin evolution is proposed during the opening of the Bakırçay graben which led to counterclockwise rotation of the Bergama block and clockwise rotation of the Dikili and Zeytindağ blocks after the early Miocene up to the Present. The rotation pattern derived from results of this study demonstrates that localized small scale deformation due to basin evolution besides regional affects must be considered as part of the deformation matrix in this area.

Keywords: Paleomagnetism; Western Anatolia; Dikili; lower Miocene volcanic rocks; Block rotation.

1. Introduction

The Alpine–Himalayan orogenic belt has experienced variable deformation along its length, reflecting both, the sizes of the colliding continental blocks and the presence of oceanic basins in proximity to orogens among other variables. The Eastern Mediterranean region is a typical example of orogenic collapse and tectonic escape. In this region, the northward subduction of the African plate beneath the Aegean region resulted in extension

of the upper crust since the Oligocene [Westaway, 1994; Faccenna et al., 2003; Taymaz et al., 2007] (Figure 1a). When the Anatolian plate collided with the Arabian Platform during the early Miocene, the East Anatolian Plateau began uplifting as a result of crustal shortening [Dewey et al., 1986; McClusky et al., 2000]. In response to subduction and continental collision, the continental crust began to escape laterally to the west of the collision front in the late Miocene–Pliocene. This tectonic escape has been accommodated by displacement along the right-lateral North Anatolian Fault Zone (NAFZ) and the left-lateral Eastern Anatolian Transform Fault Zone (EAFZ) [e.g. McKenzie, 1978; Dewey and Şengör, 1979; Le Pichon and Angelier, 1981; Taymaz 1990; Taymaz et al., 1991; McClusky et al., 2000, 2003].

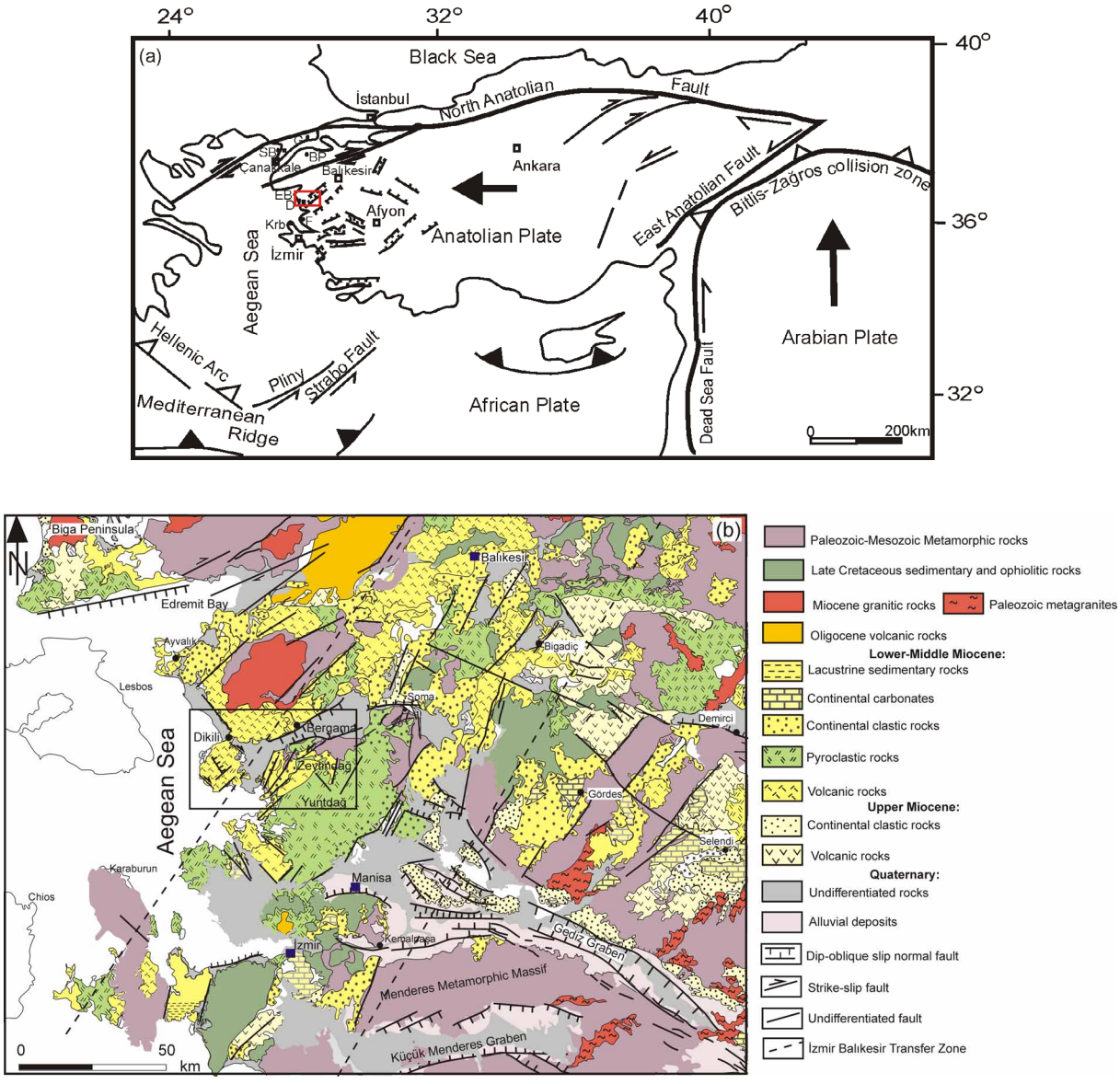

Figure 1. a) Tectonic map of the Western Anatolia Region (after Stampfli [2000]; Uzel et al. [2015]; D: Dikili, F: Foça, G: Gelibolu, BP: Biga Peninsula, EB: Edremit Bay, SB: Saroz Bay, Krb: Karaburun; study area outlined).
b) Tectonic and geological structures of the study area and its surroundings [modified after MTA, 2002]. SSW-NNE trending dashed lines designate the İzmir-Balıkesir Transfer Zone (İBTZ). Squared frame outlines paleomagnetic sampling area of Figure 2.

The northern Aegean region is affected by displacement along the NAFZ, which continues westwards into the North Aegean Trough, and splits into south bending branches in the Saros and Edremit bays [Barka and Kadinsky Cade, 1988; Taymaz et al., 1991; Barka, 1992; Kurt et al., 1999]. In contrast, the southern Aegean area is subjected to the Hellenic Zone subduction and has been deformed by displacement along the Pliny–Strabo Fault Zone [Le Pichon and Angelier, 1979; Woodside et al., 2000; Huguen et al., 2001; Piper and Perissoratis, 2003]. The Neotectonic extension in western Anatolia has been explained by tectonic escape [Dewey and Şengör, 1979; Şengör, 1979, 1980; Şengör et al., 1985; Görür et al., 1995], orogenic collapse [Seyitoğlu and Scott, 1992], slab retreat and back-arc extension [Le Pichon and Angelier, 1979; Meulenkamp et al., 1994; Okay and Satır, 2000], or an episodic two-stage extension model [Sözbilir and Emre, 1996; Koçyiğit et al., 1999; Işık and Tekeli, 2001; Lips et al., 2001; Sözbilir, 2001, 2002; Bozkurt and Sözbilir, 2004]. Velocity differences between the Aegean and Anatolian plates have been documented by geodetic studies [Doglioni et al., 2002].

The origin of Late Cenozoic magmatic activity in Western Anatolia has been debated. Two phases of volcanic activity have been documented. The older, dominantly intermediate calc-alkaline volcanic successions were followed by mafic alkaline magmatic assemblages [Yılmaz et al., 2000; Karacık et al., 2007; Dilek and Altunkaynak., 2009; Ersoy et a., 2011; Uzel et al., 2020]. Güleç [1991] showed that the lower-middle Miocene volcanic rocks were generated from a shallow mantle reservoir and modified by extensive crustal contamination, whereas the younger, upper Miocene to Quaternary volcanic rocks were generated by upwelling of an isotopically-depleted deeper mantle source, also associated with an extensional regime. Uzel et al. (2020) distinguished early Miocene calc-alkaline and shoshonitic rocks and middle to late Miocene alkaline rocks in the volcanism of the eastern Aegean region along the NE-SW striking İzmir-Balıkesir Transfer Zone (İBTZ). They reported a significant age gap in the Langhian magmatism. An alternative view suggests that volcanic activity was initiated in an extensional regime with N-S extension in the latest Oligocene-early Miocene [e.g. Seyitoğlu and Scott, 1992, Seyitoğlu et al., 1997]. A number of authors [e.g. Yılmaz, 1989, 2017] suggested that the N-S compressional regime in the early Miocene was replaced by N-S extension during the middle-late Miocene. This led to N-S trending grabens that were formed during E-W extension in the early Miocene [Yılmaz et al., 2000; Yılmaz, 2017], and E-W trending grabens that developed due to N-S extension in the late Miocene-Pliocene [Koçyiğit et al., 1999; Bozkurt, 2000, 2003].

Several paleomagnetic studies deal with the reconstruction of crustal blocks due to the activity of the North Anatolian Fault over the past [Piper et al., 1996; 1997; 2010; Gürsoy et al., 2011; Tatar et al., 2013]. Previous studies in western Anatolia reported different senses of rotations, either during or after the extensional phase during the Miocene [Kaymakçı et al., 2007; Uzel et al., 2017]. Counterclockwise rotations have been observed in upper Oligocene, lower-middle and upper Miocene volcanic rocks in Western Anatolia, in the area between Çanakkale, Foça and Bergama (Figure 1a,b) by Orbay et al. [1998] and İşseven et al. [1995]. These authors, however, infer no significant rotation in the north of Biga Peninsula (Figure 1a,b), but inclination discrepancies were postulated as a result of tilting related to listric faulting [Orbay et al., 1998; İşseven et al., 1995]. In Karaburun and Izmir, Lauer [1984] reported data suggesting clockwise and counterclockwise rotations, yet Orbay et al. [2001] reported data suggesting clockwise rotations in this region. Counterclockwise rotation of between 20° and 30° was inferred for the entire Anatolian plate in a study by Platzman et al. [1998] and Kissel et al. [2003]. Van Hinsbergen et al. [2010] used previously published paleomagnetic data to analyse the regional tectonic structures and proposed that oroclinal bending affected Western Anatolia. They documented a counterclockwise rotation of ~20° for the Lycia nappe and Beydağları autochthon between 16 and 5 Ma. This rotational phase was interpreted to coincide with the exhumation of the Central Menderes Massif [van Hinsbergen 2010; Figure 1a,b] in the late Oligocene-Miocene. In the area between Lesbos Island and Uşak, no significant rotation took place since the Miocene, although significant clockwise rotation of ~20° was reported between this area and Afyon. The study of Uzel et al. [2015], however, concluded that there were two phases of rotation, in the early Miocene and in the late Miocene, based on the lateral displacement, first sinistral and then reactivated as dextral, along the İzmir-Balıkesir Transfer Zone (İBTZ, Figure 1a,b) across Bergama and Söke [Uzel et al., 2017].

For this study, we sampled 35 sites in the lower Miocene volcanic rocks of the Bergama, Zeytindağ and Dikili subareas of Western Anatolia and combined our results with previous data from the study area to unravel possible block rotations. Although previous studies have interpreted any paleomagnetic data in the framework of large scale crustal deformation, the focus of our investigation concentrates on differential rotation and small block displacement that may have affected this area.

2. Geologic setting

The study area is characterized by NE-SW trending normal faults, displacement along which graben and horst blocks, such as the Bergama-Dikili graben and the Kozak Horst, formed [Karacık et al., 2007; Hou et al., 2015]. The active fault zones in the study area are the NE-SW oriented left lateral Zeytindağ-Bergama Fault zones (Figure 2). The NW-SE Dikili graben is the most important tectonic feature in the study area and represents the western extension of the V-shaped 60 km long Bergama graben [Yılmaz et al., 2000]. A series of E-W trending normal faults merge within the graben system, providing evidence of a N-S extension regime in the area.

Our research is concentrated on the crustal elements, the Bergama, Zeytindağ and Dikili blocks (Figure 2). The Bergama block is confined along its southern margin by the NW-SE Dikili depression, by the NW directed Altınova Fault to the west and the NE-SW striking Bergama Fault and Kıranlı Fault to the east (Figure 2b). The Kozak horst is located to the north of the Bergama block. Farther southwest, the Dikili block is confined by the Çandarlı Fault on its southeastern edge with a number of small strike-slip faults to the north. The whole area from the north to the southeast is surrounded by several graben structures. To the east, the Zeytindağ block is delimited by grabens to the N-NE and the Zeytindağ horst to the SE. The Kaşıkçı and Turgut-Özalp faults continue to the northeast. Dip slip normal faults, displacing horsts versus grabens, are the main tectonic features. They are also responsible for rotational motions, which resulted from N-S extension of the study area (Figure 2).

Sangu et al. [2020] described three NE-trending highs in the Bergama region that are bounded by normal faults having NE and NW trending strike slip displacement components. Active faults in the region form large bends with E–W orientation and southward concavity, beginning along the Zeytindağ Fault Zone towards the east in Western Anatolia [Emre et al., 2018]. Sangu et al. [2020] designated the NE-trending Yenikent-Bergama and Çandarlı Fault Zones as major faults at a scale of less than 15 km around Bergama, Yuntdağ and Dikili and argued the Bergama and Kınık-Turgutalp fault zones - as normal dextral strike slip faults - to be the southernmost branches of the NAFZ. Westerweel et al. [2020] reported that faults observed within the Soma basin, which lies to the east of the study area, can be classified into three general groups: NE-SW trending dextral strike-slip faults with high dip angles, NW-SE trending sinistral strike-slip faults with a larger normal component, and E-W trending normal faults.

The stratigraphy of the study area is defined at the base by metamorphic Paleozoic rocks which were metamorphosed during the latest Triassic [Bingöl et al., 1973; Akyürek and Soysal, 1983; Koçyiğit, 1987; Genç and Yılmaz, 1995; Altıner and Koçyiğit, 1993; Altunkaynak, 1996]. Metamorphic, plutonic, volcanic and sedimentary rocks crop out north of the Kozak horst [Bingöl et al., 1982]. The volcanic and associated sedimentary rocks are of Neogene age (Figure 3). Volcanic rocks are the most common rocks exposed and include pyroclastic rocks, lava flows with the associated sedimentary or volcanoclastic rocks of the Ballıca/Soma formation and the upper Miocene–Pliocene Zeytindağ Group, which consists of rhyolitic domes and basaltic andesite-basalt lavas and dikes [Aldanmaz et al., 2000; Karacık et al., 2007; Sangu et al., 2020].

Yılmaz et al. [2000] assigned the lower-middle Miocene volcanic rocks in the study area to the Dikili Group, which comprises a 750 m thick sequence that overlies unconformably Paleozoic metamorphic rocks. Near the base, the sequence includes dark siltstones, purple mudstones, and bituminous shales. The volcanic rocks, spatially and temporally associated with the sedimentary rocks of the Dikili Group, are predominantly andesite, latite, dacite lavas and their pyroclastic equivalents [Karacık et al., 2007]. Numerical age data on the andesite and dacite lavas range from 19 to 15 Ma [Ercan et al., 1985; Altunkaynak and Yılmaz, 1998, and references therein]. Palaeontologic data from intercalated sedimentary rocks imply early-middle Miocene ages [Akyürek and Soysal, 1983; Ercan et al., 1985]. The upper Miocene–Pliocene Zeytindağ Group begins with internally-chaotic coarse grained detrital rocks that grade upwards into sandstones, siltstones, mudstones, marls and white lacustrine limestones. Andesitic volcanic activity had evidently waned before the development of the northeast-southwest trending grabens because the sedimentary fill is devoid of intermediate composition volcanic rocks. Only a few, scattered basaltic lava flows were erupted during this time. These are interbedded with lacustrine limestones of late Miocene Ballıca/Soma Formation [Nebert, 1978; Akyürek and Soysal, 1983; Ercan et al., 1985]. The lavas were fed from fissures, associated mainly with NE-SW graben-bounding faults, and their Rb/Sr age has been estimated at 9 to 6 Ma [Borsi et al., 1972; Ercan et al., 1985]. The contact between the Dikili and Zeytindağ groups has been shown to be an unconformity [Karacık et al., 2007].

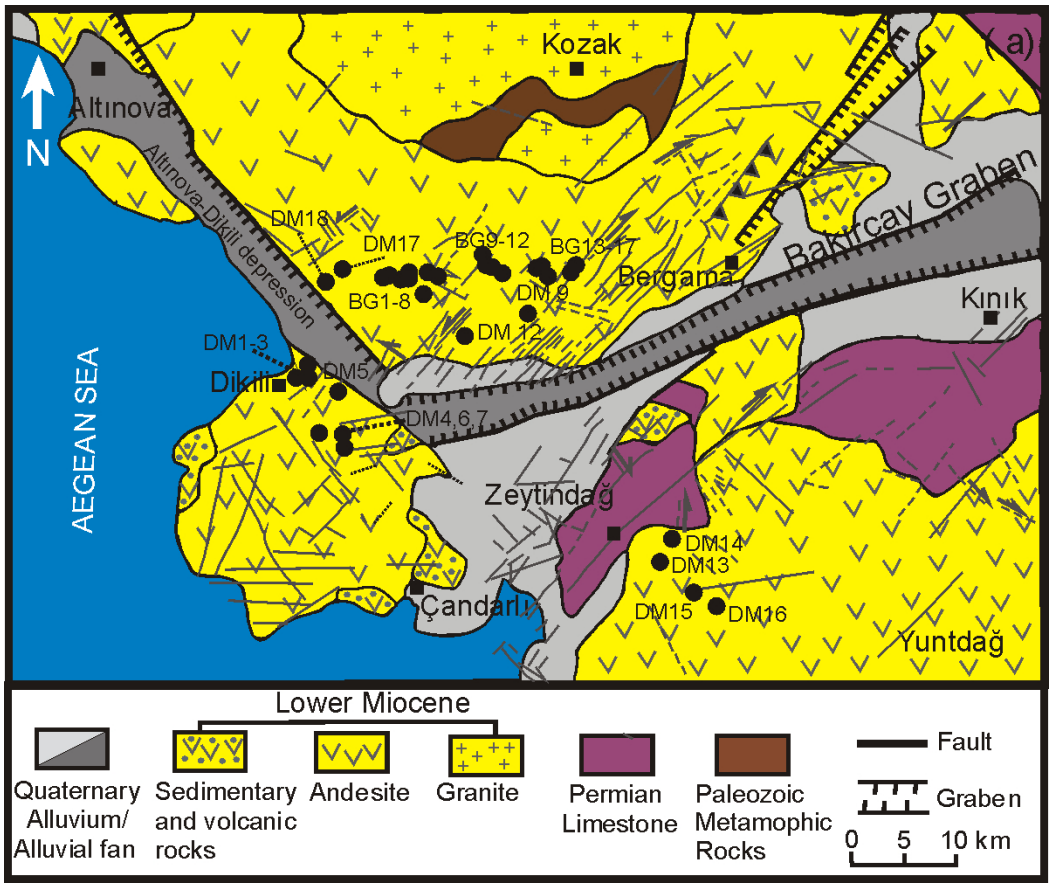

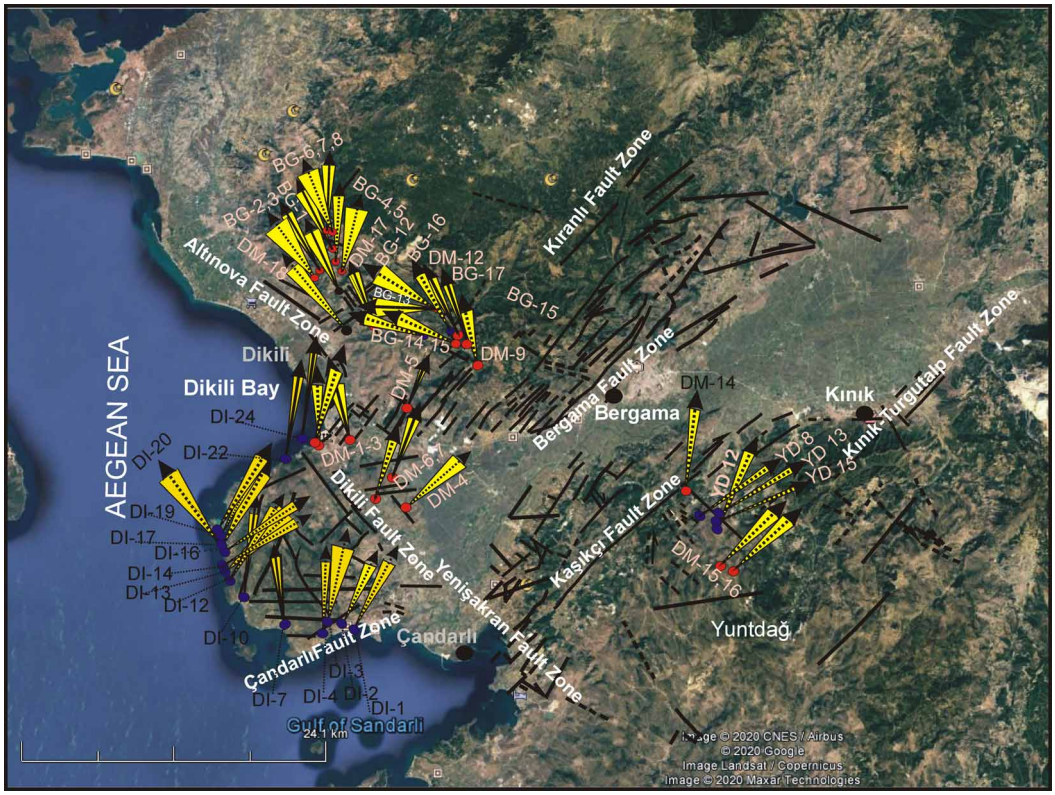

Figure 2. a) Geological map of the study area with paleomagnetic sampling sites [after Altunkaynak and Yılmaz, 1998, 1999]. b) Rotated paleomagnetic declinations obtained from sites of this study (red circles) and of previous studies (blue circles). The fault zones have been named by Sangu et al. [2020].

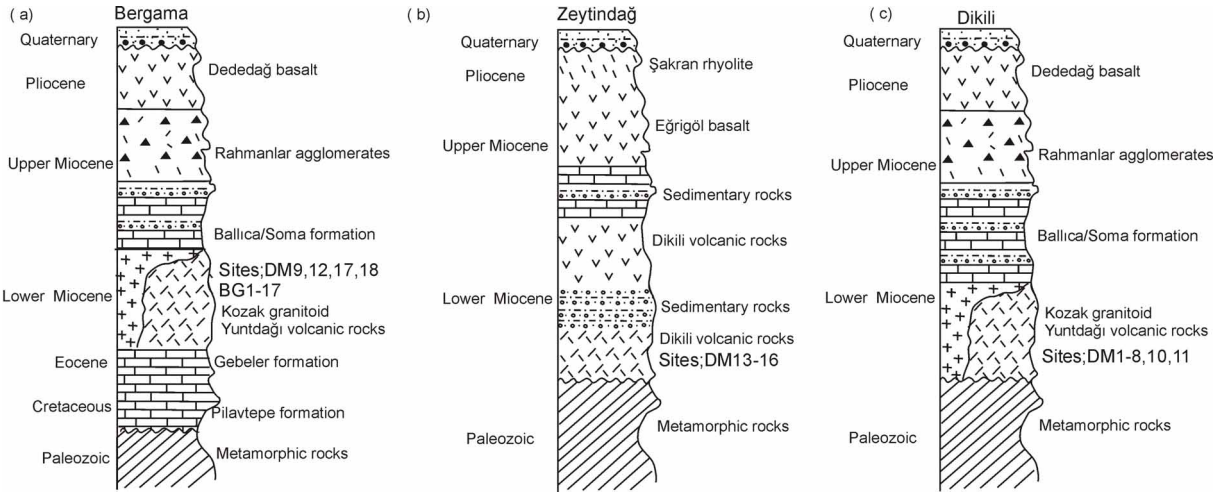

Figure 3. Stratigraphic sections from the a) Bergama [Akyürek and Soysal, 1983], c) Zeytindağ [Karacık and Yılmaz, 2000] and c) Dikili [Akyürek and Soysal, 1983] sub-areas, showing the levels sampled by this paleomagnetic study.

3. Paleomagnetic sampling and methods

Sampling for the paleomagnetic study focused on lower Miocene volcanic rocks of the Yuntdağ sequence which are distributed over three subareas around Bergama, Zeytindağ and Dikili (Figure 2). This volcanic sequence consists mainly of pyroclastic deposits and flows. The pyroclastic deposits are medium-sized to coarse-grained ignimbrites of andesitic and latitic composition. They are intercalated with a lower sedimentary sequence [Karacık and Yılmaz, 1998; Genç et al., 2001]. Lavas of the Dikili Group are of early to middle Miocene age [16.7 – 18.5 Ma: Borsi et al., 1972; Benda et al., 1974; 15.2 ± 0.40 – 15.5 ± 0.30: Aldanmaz et al., 2000]. We sampled andesitic volcanic rocks at 35 sites: twenty one sites (DM9,12,17,18, BG1-17) were obtained from the Bergama block (Figures 2, 3a), four sites (DM13-16) were sampled on the Zeytindağ block and ten sites (DM1-8,10,11) were collected in the Dikili block. In addition, outcrops were separated by tens to more than hundreds of metres at different elevations to avoid multiple sampling the same volcanic unit.

A motorized portable drill was used to collect orientated independent core samples. Drill cores of 2.5 cm diameter were cut into 2.2 cm long cylindrical specimens. Sample orientation was determined using both magnetic and sun compasses.

A total of 250 specimens was subjected to both stepwise thermal and alternating field (AF) demagnetization. The directions and intensities of the natural remanent magnetization (NRM) were measured using a JR-6 spinner magnetometer (AGICO) in the Yılmaz Ispir Paleomagnetism Laboratory of Istanbul University-Cerrahpaşa, Turkey. Both thermal and alternating field demagnetizations were applied to isolate the characteristic remanent magnetizations (ChRM) in steps between 50° C and 700° C, using a Magnetic Measurements MTD-80 oven, or 2.5 and 150 mT, using a 2G600 AF demagnetizer, respectively. Magnetization components were identified and calculated using orthogonal vector projections [Zijderveld, 1967]. The directions of individual NRM components were calculated using principal component analysis [Kirschvink, 1980]. Fisher's [1953] statistics were used to calculate site mean directions and their angular dispersion. To test the angular standard deviation of the virtual geomagnetic poles of the data in order to check for adequate averaging of the geomagnetic field, we used the criteria developed by Deenen et al. [2011]. These criteria are statistically expressed by polar A_{95} confidence limits (A_{95}max and A_{95}min), and the number of sites (N) per subarea. Fold tests after McElhinny [1964] and McFadden [1990] together with the reversal test of McFadden and McElhinny [1990] were applied to evaluate the ChRM ages in the context of the regional deformation. Temperature-dependent low field susceptibility of 35 representative samples was measured by heating in air, using an MS2 Bartington susceptibility meter. Isothermal remanent magnetization (IRM) was induced for one specimen per site by applying fields up to 1 T along the Z-axis with an ASC pulse magnetizer.

Coercivity spectra were tested by applying fields of 1 T along the sample Z-axis (hard component), 0.4 T (medium component) along the Y-axis, and 0.12 T (soft component) along the X-axis (Lowrie, 1990). Subsequently, these samples were thermally demagnetized to identify the magnetic carriers, based on their thermal unblocking behavior. Anisotropy of magnetic susceptibility (AMS) was measured with a Bartington magnetic susceptibility meter (MS2 & MS2B system). Eigenvalues ($\kappa_1 \geq \kappa_2 \geq \kappa_3$) and principal axes directions of the AMS ellipsoid were calculated with the Bartington software package. Mean AMS eigenvectors and their 95% confidence limits were calculated using the methods of Jelinek [1977; 1978].

4. Rock magnetic results

Rock magnetic results suggest that the volcanic rocks can be divided into three types of magnetic assemblages. Most samples are characterized by nearly reversible susceptibility curves during heating and cooling, indicating a single ferrimagnetic phase with Curie temperatures between 550 and 580° C, most probably Ti-poor titanomagnetite (Figure 4a1). These mineral phases have low coercivity, and their IRM is saturated below 200 mT (Figure 4a2). High coercivity minerals are virtually absent in the 3-component IRM demagnetization curves (Figure 4a3), but maximum unblocking temperatures of the soft and dominating IRM component above 600° C show at least partial oxidation of titanomagnetite. The second type of behavior also shows quasi-reversible curves but with weaker susceptibility and Curie temperatures well above 600° C (Figure 4b1). The IRM is not saturated by a 1T applied field and only negligibly magnetized in fields below 200 mT (Figure 4b2,3). Therefore strongly oxidized magnetic material, probably hematite, is present with maximum unblocking temperatures of the high coercivity IRM component above 650° C, and in addition minor amounts of titanomaghemite. The latter may be responsible for the relatively high low field susceptibility. A third magnetic rock type is characterized by a weaker susceptibility than that found in the first category (Figure 4c1), but with an IRM that saturates in an applied field of about 300 mT (Figure 4c2). The corresponding magnetic mineral phase may be represented by fine-grained titanomaghemite of intermediate composition. Upon heating, susceptibility (Figure 4c1) increases at first up to 220° C. This behaviour is interpreted as unblocking of single-domain ferrimagnetic grains attaining superparamagnetic behaviour. The inflexion below 400° C indicates the Curie temperature of pristine maghemite material which alters upon heating so that an apparent Curie temperature is observed above 615° C, being similar to the maximum unblocking temparatures of the soft IRM component in Figure 4c3.

Consistent AMS fabric data have been obtained at 35 sites, with magnetic susceptibility values (κ_m) ranging between 10^{-3}–10^{-2} SI, indicating the predominance of magnetite as observed in the rock magnetic experiments. Lava flows tend to be foliated as recognized by well-grouped clustering of κ_{min} axes either parallel or perpendicular to the flow contacts, and κ_1 axes typically are in the flow plane. In the P-U diagram [Jelinek, 1981], ellipsoid shapes are mainly oblate ($T > 0$; Figure 5 and Figure 6). Lineation data, as expressed by the L parameter (κ_1/κ_2), range from 1.005 to 1.08, whereas foliation, as expressed by the F parameter (κ_2/κ_3), ranges between 1.00 and 1.06. The P values (κ_1/κ_3) are between 1.03-1.12, and T values are almost exclusively positive (Appendix A). The directions of maximum susceptibility axes (κ_1) may define the orientation of lava flow directions [Knight and Walker 1988; Archanjo et al., 2000; Herrero-Berrera et al., 2001; Gil et al., 2002; Ellwood, 1978; Canon-Tapia et al., 1996; Geoffroy et al., 2002]. The maximum susceptibility axes generally plunge with less than 45° relative to flow contacts, suggesting lava flow deformation by simple shear [Loock et al., 2008]. The regionally highly variable and unsystematically distributed AMS axes directions imply that the volcanic rocks have not been deformed internally after emplacement.

5. Paleomagnetic Results

NRM components with intensities in the range of 200-5000 mA/m are isolated during AF and thermal demagnetization (Figure 7). Demagnetization shows a main ChRM component that decays to the projection origin for most specimens after removal of a viscous component. The viscous component is removed between 75° C and 150° C (Figure 7b, e) or 5 and 10 mT (Figure 7f, j). The ChRM directions of almost all specimens were isolated up to laboratory unblocking temperatures of 500° C to 580° C or at higher AF values (> 20 mT). Several volcanic samples have been unblocked between 600° C and 625° C (Figure 7a) due to the frequent presence of oxidized

ferromagnetic minerals such as titanohematite or maghemite as remanence carriers observed in the thermomagnetic curves (Figure 4).

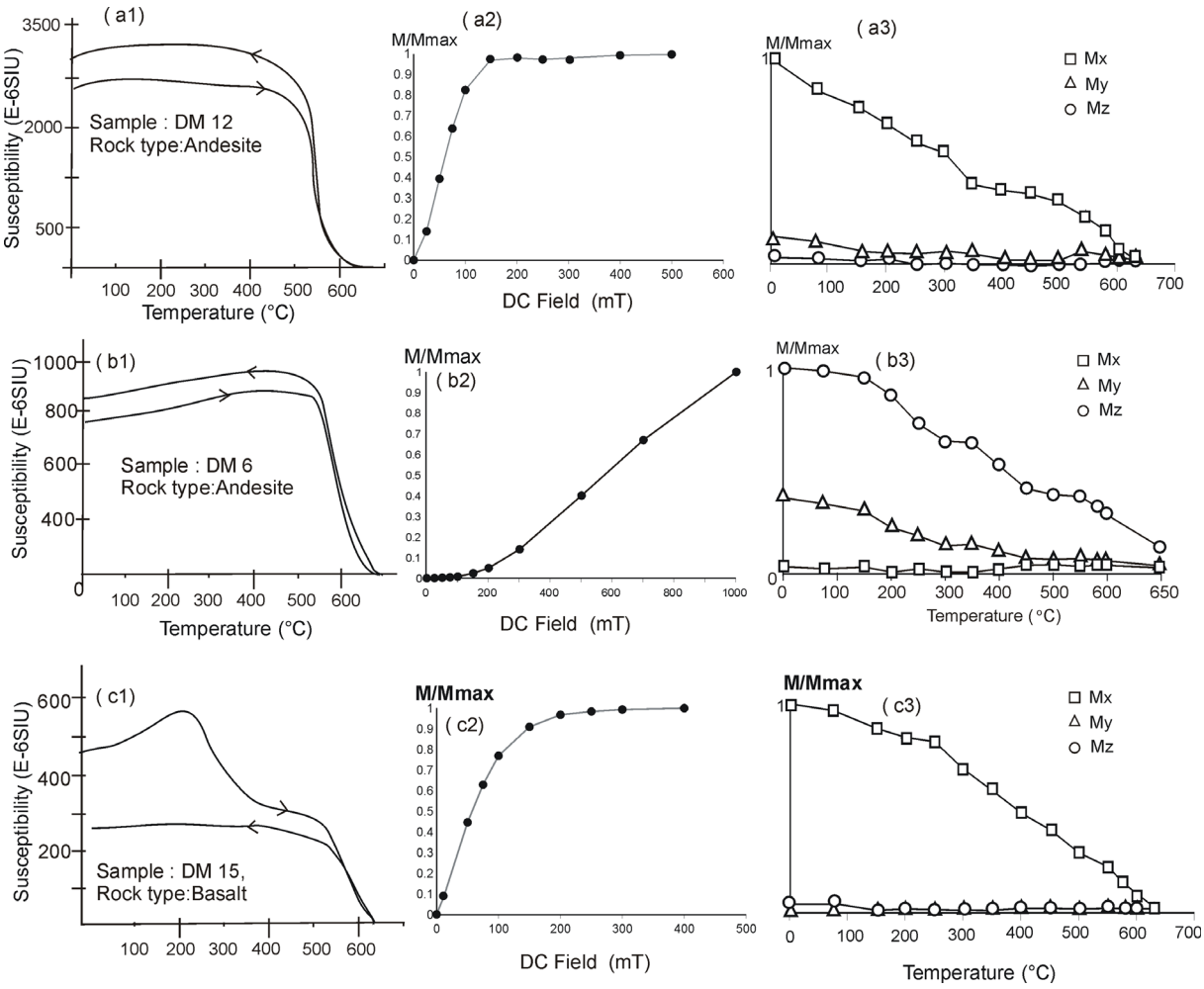

Figure 4. Thermomagnetic susceptibility curves of representative samples indicating the occurrence of titanomagnetite (a1, b1, c1) in variable oxidation states. Normalized IRM curves (a2, b2, c2) and thermal demagnetization of three-axial IRM (a3, b3, c3; hard M_z, medium M_y, and soft M_x). High coercivity hematite is observed in andesite sample DM6.

5.1 Paleosecular Variation

Palaeosecular variation (PSV) describes the long-term average behavior of the geomagnetic field and can be estimated if a sufficient number of short-term, essentially instantaneous determinations represented by virtual geomagnetic poles (here site readings from individual lava flows) can be averaged. It is described by the angular standard deviation of these discrete virtual determinations (S_W) and the total angular dispersion (S_P) of N virtual geomagnetic poles (VGP) is defined using the formula

$$S_p = \left(\frac{1}{N-1}\sum_{i=1}^{N} \Delta_i^2\right)^{1/2}$$

where Δ is the angular distance between the ith VGP and the spin axis [McElhinny and McFadden, 1997]. The dispersion (S_F) produced by paleosecular geomagnetic field variations is derived by subtracting the within-flow circular standard deviation of the VGP (S_W), which is generally very small, from S_P. It arises from the random errors in the paleomagnetic direction at the corresponding site and has been estimated by Cox [1969] as

$$S_F^2 = S_P^2 - S_W^2/N$$

[cf. also PMAG Software, Tauxe, 1998]. If the A_{95} angle calculated for a mean VGP lies between the lower (A_{95}min) and upper (A_{95}max) boundaries, the observed VGP population scatter is inferred to average out PSV. Our investigated lava flows were emplaced over a sufficient time interval of both normal and reverse geomagnetic field polarity and average out PSV on all of our three blocks studied (Table 1). As noted above, outcrops were separated from tens of metres to more than hundreds of metres at different elevations to avoid sampling the same volcanic unit multiple times. All of our localities yield A_{95} values that lie within the reliability envelope (Table 1).

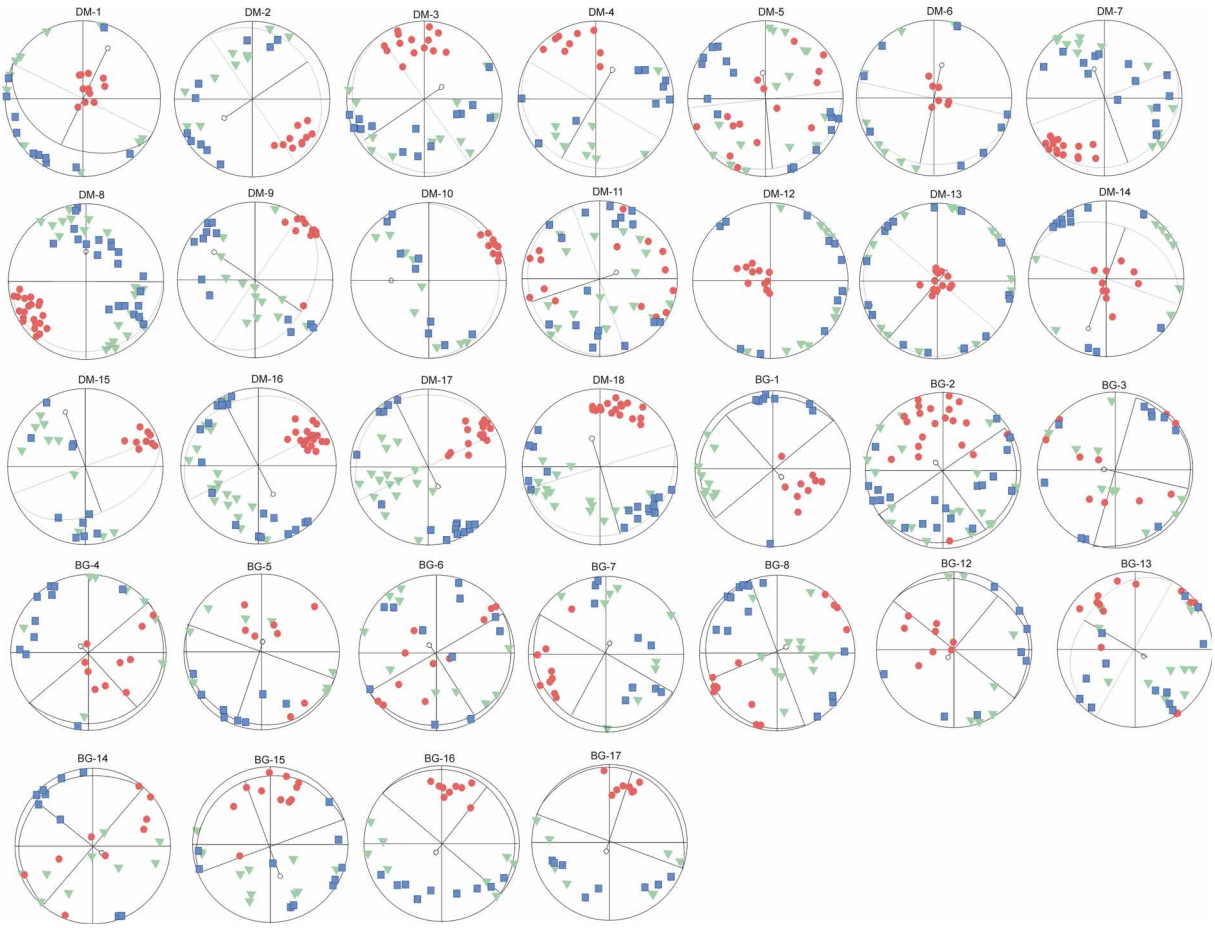

Figure 5. Stereographic projection of the principal susceptibility axes in geographic coordinates. Black traces of great circles represent bedding plane orientation if not horizontal. Blue squares, green triangles and red circles represent maximum, intermediate, and minimum axes of the anisotropy ellipsoid, respectively.

Site	N/n	Latitude	Longlitude	Strike/Dip	D_g	I_g	D_s	I_s	k	α_{95}
GROUP 1 Bergama Block										
DM9	9/9	39.00877	26.98106	124/41	352.0	4.9	341.0	33.4	128.12	4.6
DM12	9/9	38.07112	26.97645	210/12	157.2	-45.4	151.4	-35.5	105.67	5.0
DM17	9/7	39.09959	26.91827	333/17	131.1	-42.4	147.5	-46.5	174.95	4.6
DM18	8/6	39.08100	26.90338	164/23	145.7	-39.5	131.2	-29.4	130.33	5.9
BG1	10/9	39.14682	26.95115	320/20	337.7	33.0	348.1	25.1	63.6	6.5
BG2	9/9	39.15020	26.95769	145/20	329.7	36.7	314.9	35.7	106.8	5.0
BG3	10/8	39.15350	26.96398	105/10	143.4	-33.2	137.4	-39.0	62.2	6.6
BG4	9/7	39.15503	26.97209	140/15	191.1	-36.9	181.6	-47.8	56.1	9.0
BG5	9/8	39.15470	26.97485	200/10	183.2	-32.5	177.6	-29.1	145.7	4.6
BG6	10/8	39.15196	26.97956	150/20	332.9	34.3	319.5	32.9	66.4	6.8
BG7	9/9	39.14720	26.98371	210/25	1.9	53.6	341.4	37.7	66.6	6.4
BG8	10/8	39.14587	26.98803	250/20	153.5	-48.7	155.1	-28.8	53.3	8.3
BG9	8/8	39.14143	26.99764	210/15	-	-	-	-	-	-
BG10	8/8	39.14585	26.99608	210/15	-	-	-	-	-	-
BG11	8/8	39.14261	27.00305	210/15	-	-	-	-	-	-
BG12	9/9	39.13011	27.03163	40/25	123.3	-11.4	121.9	-36.2	50.2	7.3
BG13	10/6	39.12914	27.04034	300/35	275.3	30.8	299.9	39.0	137.0	5.7
BG14	8/8	39.12922	27.04116	310/20	106.9	-36.6	122.9	-41.9	81.7	6.2
BG15	9/9	39.12325	27.04045	340/25	114.4	-12.9	121.8	-29.8	63.4	6.5
BG16	9/9	39.12329	27.05370	40/20	152.3	-34.8	161.0	-52.8	99.2	5.2
BG17	10/10	39.12420	27.06199	20/10	340.5	41.0	348.4	46.8	133.9	4.2
Mean DM9,12,17,18; BG1-8,12-17; N:18					327.7	36.7			10.8	11.0
							326.9	38.7	21.6	7.6
							A_{95} = 14.7, A_{95min} = 6.9, A_{95max} = 34.2			
GROUP 2 Zeytindağ Block										
DM13*	-	38.95115	27.22505	166/12						
DM14	12/12	38.97552	27.17314	20/45	141.2	-34.3	186.8	-63.9	372.63	2.3
DM15	8/7	38.93446	27.20994	0/50	171.6	-48.5	218.0	-33.8	86.31	6.5
DM16	10/8	38.93351	27.21454	333/25	18.1	55.3	34.0	35.1	69.56	6.7
YD2[a]*	6	38,9686	27.1780	H	198.1	-8.7	198.1	-8.7	96.7	6.2
YD8[a]	7	38,9417	27.1930	H	234.5	-65.8	234.5	-65.8	1499.3	1.6
YD12[a]	6	38,9420	27.2081	H	203.4	-29.5	203.4	-29.5	367.5	3.5
YD13[a]	6	38,9499	27.2042	H			247	-38.5	8657.8	0.7
YD15[a]	7	38,9575	27.2041				238.5	-37.1	1643	1.5
Mean DM13-16; YD8,12,13,15; N:7					204.5	-50.3			7.4	23.7
							221.3	-44.8	15.7	15.7
							A_{95} = 17.4, A_{95min} = 5.5, A_{95max} = 24.1			
GROUP 3 Dikili Block										
DM1	15/14	39.05457	26.88541	206/48	228.0	-44.7	178.4	-42.0	238.3	2.6
DM2	1818	39.06506	26.89801	56/26	344.9	-4.5	346.2	20.1	52.88	4.8
DM3	25/25	39.08027	26.90606	235/16	203.2	-43.6	192.9	-33.9	79.11	3.3
DM4	14/14	39.07925	26.90595	210/27	201.7	-27.5	189.7	-20.6	77.13	4.6
DM5	16/16	39.07017	26.90832	175/20	39.5	40.2	22.4	52.2	344.31	2.0
DM6	20/20	39.03304	26.91038	192/26	39.0	32.1	20.5	40.3	80.39	3.7
DM7	15/15	39.03191	26.90771	160/23	218.6	-45.0	197.2	-62.5	197.5	2.7
DM8*	-	39.00722	26.90999	180/23	-	-	-	-	-	-
DM10*	-	39.03332	26.97900	90/20	-	-	-	-	-	-
DM11*	-	39.08762	26.93311	250/13	-	-	-	-	-	-
DI1[a]	7	38.9306	26.8941	H	207.5	-24.1	207.5	-24.1	423.3	2.9
DI2[a]	6	38.9297	26.8924	H	203.9	-32.5	203.9	-32.5	339.5	3.6
DI3[a]	6	38.9283	26.8894	H	191.6	-63.4	191.6	-63.4	92.5	6.3
DI4[a]	6	38.9263	26.8903	H	181.8	-56.4	181.8	-56.4	1323	1.8
DI5[a]*	7	38.9284	26.8788	H	32.9	-33.2	32.9	-33.2	167.8	4.7
DI6[a]*	7	38.9301	26.8751	H	325.2	20.8	325.2	20.8	765.1	2.2
DI7[a]	7	38.9315	26.8678	H	352.9	73.8	352.9	73.8	498.2	2.7
DI8[a]*	7	38.9350	26.8606	H	211.1	18.1	211.1	18.1	46.3	9
DI9[a]*	7	38.9374	26.8566	H	298.3	-21	298.3	-21	185.8	4.4
DI10[a]	7	38.9463	26.8336	H	7.1	36.9	7.1	36.9	254.4	2.5
DI11[a]*	7	38.9564	26.8152	H	208.9	5.6	208.9	5.6	620.3	2.4
DI12[a]	7	38.9573	26.8088	H	211.9	-25.7	211.9	-25.7	1194.9	1.7
DI13[a]	7	38.9686	26.8024	H	226.7	-35	226.7	-35	52.1	8.4
DI14[a]	7	38.9698	26.8017	H	240	-27.1	240	-27.1	1142.1	1.8
DI15[a]*	7	38.9783	26.8026	H	299	-24.3	299	-24.3	72	7.2

DI16[a]	7	38.9801	26.8021	H	237.1	-25.6	237.1	-25.6	720	2.3
DI17[a]	7	38.9823	26.8010	H	209.3	-28.3	209.3	-28.3	93	6.3
DI18[a]*	7	38.9842	26.7994	H	143.8	-47.9	143.8	-47.9	55.7	8.2
DI19[a]	7	38.9855	26.7986	H	209	-35	209	-35	276.4	3.6
DI20[a]	7	38.9848	26.7995	H	211.7	-38.6	211.7	-38.6	137.2	5.2
DI21[a]*	7	39.0328	26.8572	H	278.5	-11.9	278.5	-11.9	178.6	4.5
DI22[a]	7	39.0346	26.8362	H	9.4	15.7	9.4	15.7	625.9	2.4
DI23[a]*	7	39.0447	26.8427	H	326.9	21.4	326.9	21.4	72.9	7.1
DI24[a]	6	39.0481	26.8451	H	8.2	15.2	8.2	15.2	1677.6	1.6
DI25[a]*	7	39.0545	26.8506	H	241.7	-4.9	241.7	-4.9	549.7	2.6
Mean DM1-7; DI1-4,7,10,12-14,16,17,19,20,22,24; N:22					206.8	-36.1			12.7	9.1
							201.1	-37.9	13.7	8.7
							A_{95} = 8.6, A_{95min} = 3.5, A_{95max} = 11.7			

Table 1. Paleomagnetic results from the Western Anatolian volcanics for the three blocks Bergama, Zeytindağ and Dikili. Columns from left: Site names, sample numbers (N denotes number of samples per locality, n the number of samples used for site mean calculation.), geographic cordinates (lat°N, long°E), bedding attitudes (H corresponds to horizontal position), declination $D_{g(s)}$ and inclination $I_{g(s)}$ describe the mean directions in geographic (before tilt correction) and stratigraphic coordinates (after tilt correction), respectively; *k* the precision parameter [Fisher, 1953], α_{95} the 95% confidence circle, A_{95} defines the angle of confidence of the VGP of each block, A_{95}min, A_{95}max are the minimum, maximum values of A_{95}, after Deenen et al. [2011]. Sites with asterisk (*) were not considered for tectonic interpretation for reasons given in the text. Sites YD and DI shown with ([a]) were considered following Van Hinsbergen et al. [2010]. Bold figures of N denote the number of sites per block used when calculating the stratigraphic block mean directions.

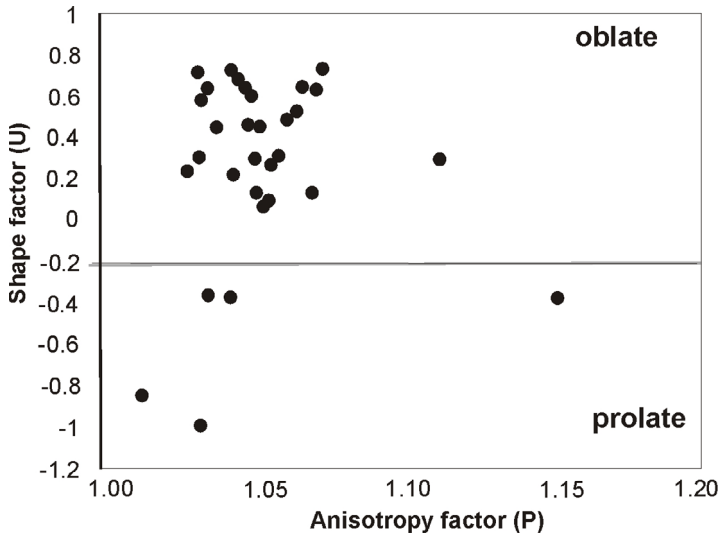

Figure 6. Anisotropy site mean shape parameter (U) versus degree of anisotropy (P).

5.2 Paleomagnetic Mean Directions

Our paleomagnetic results and the previous dataset reported by van Hinsbergen et al. [2010] were compiled to evaluate the possibilities of different senses of rotations (Figure 2b) among the three inferred structural areas. These data are used to calculate a group mean direction for each area, referred to as Groups 1, 2 and 3.

The mean direction of Group 1 (Bergama Block) is D = 326.9° and I = + 38.7° (*k* = 21.6, α_{95} = 7.6°, N:18 sites) in stratigraphic coordinates, with seven normal and eleven reverse polarity sites (Table 1, Figure 8a, d).

Anomalous demagnetization behavior was observed at sites BG 9,10,11 and these results were not considered in farther interpretation. The precision parameter increases to a value of $k_s/k_g = 2.0$ and critical angular values at 95% = 1.78 and 99% = 2.26, at the 95% confidence level in the McElhinny [1964] fold test. When applying the progressive fold test of McFadden [1990], a maximum k value is obtained at 110% unfolding, suggesting a pre-folding magnetization. A positive reversal test is obtained with classification "C" [McFadden and McElhinny, 1990]; the observed angular distance $g_o = 4.0°$ is less than the critical angle $g_c = 16.5°$ (normal polarity $N = 7$, resultant vector of length $R = 6.7$ and $k = 23.3$ and reversed polarity N = 11, resultant vector of length $R = 10.4$ and $k = 17.8$).

Group 2 (Zeytindağ Block) has a mean ChRM of D = 221.2°, I = -44.8° ($k = 15.6$, and $\alpha_{95} = 15.8°$, N = 7) in stratigraphic coordinates with one site of reverse polarity and six of normal polarity (Table 1, Figure 8b). Site YD2 from van Hinsbergen et al. [2010] is excluded from the mean direction due to a very shallow inclination, and no interpretable results could be obtained from site DM 13.

Group 3 (Dikili Block) is characterized by seven sites of normal polarity and 15 of reverse polarity that yield a mean direction of D = 201.0°, I = -37.9° ($k = 13.6$ and $\alpha_{95} = 8.7°$, N = 22) in stratigraphic coordinates (Table 1 and Figure 8c). Several sites have not been considered in the calculation of a mean direction of this group because no interpretable results could be identified during demagnetization (DM8, 10, 11) or because these exhibit very high dispersion (sites DI5,6,8,9,11,15,18,21,23,25). Seven site mean directions from normal polarity sites (resultant vector of length $R = 6.5$ and $k = 11.6$) and fifteen of reverse polarity (resultant vector of length $R = 14.2$ and $k = 16.7$) show an observed angular distance $\gamma_o = 16.5°$, which is less than the critical angle $\gamma_c = 18.1°$ [cf. McFadden, 1990], thus showing a positive reversal test with "C" classification. A reliable fold test could not be performed on data from Groups 2 and 3, because tilted lavas - bedding varying between 0° and 48° - were included only in the present study whereas the previous study only sampled horizontal lava flows.

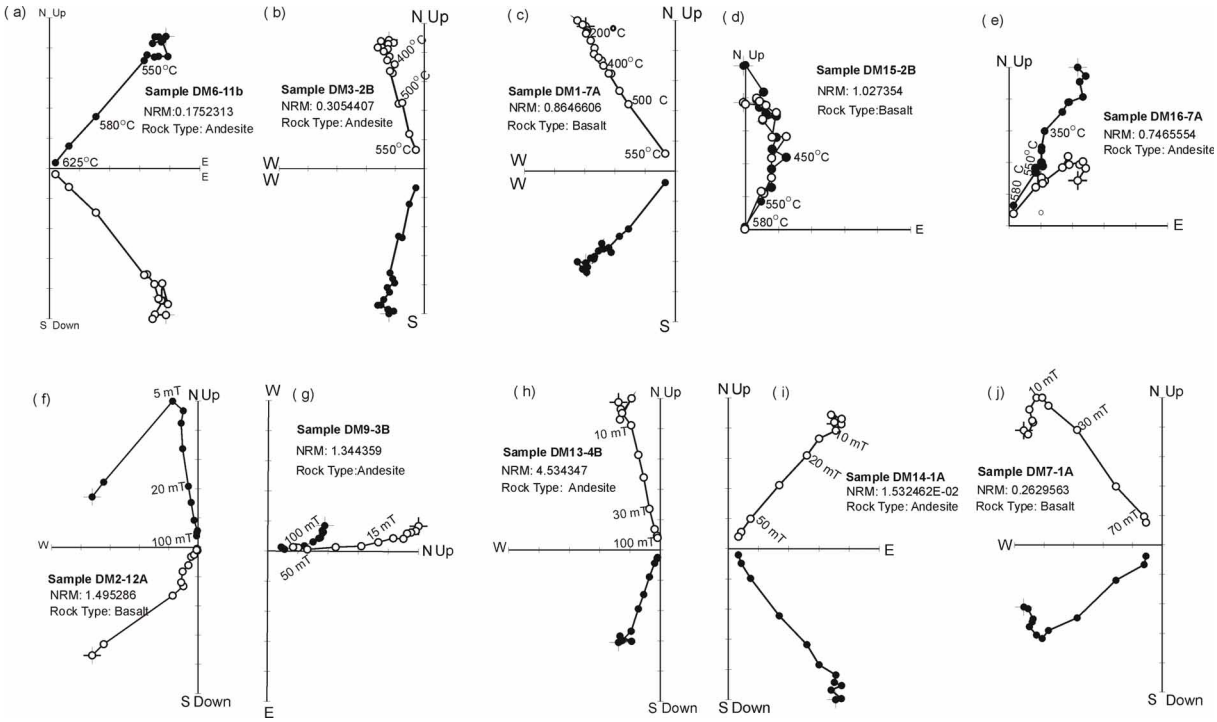

Figure 7. Zijderveld [1967] diagrams in stratigraphic coordinates of representative samples during stepwise thermal and alternating field demagnetization (in centigrades and mT, respectively). NRM intensities in Am^{-1}. Solid (open) symbols for horizontal (vertical) components, respectively.

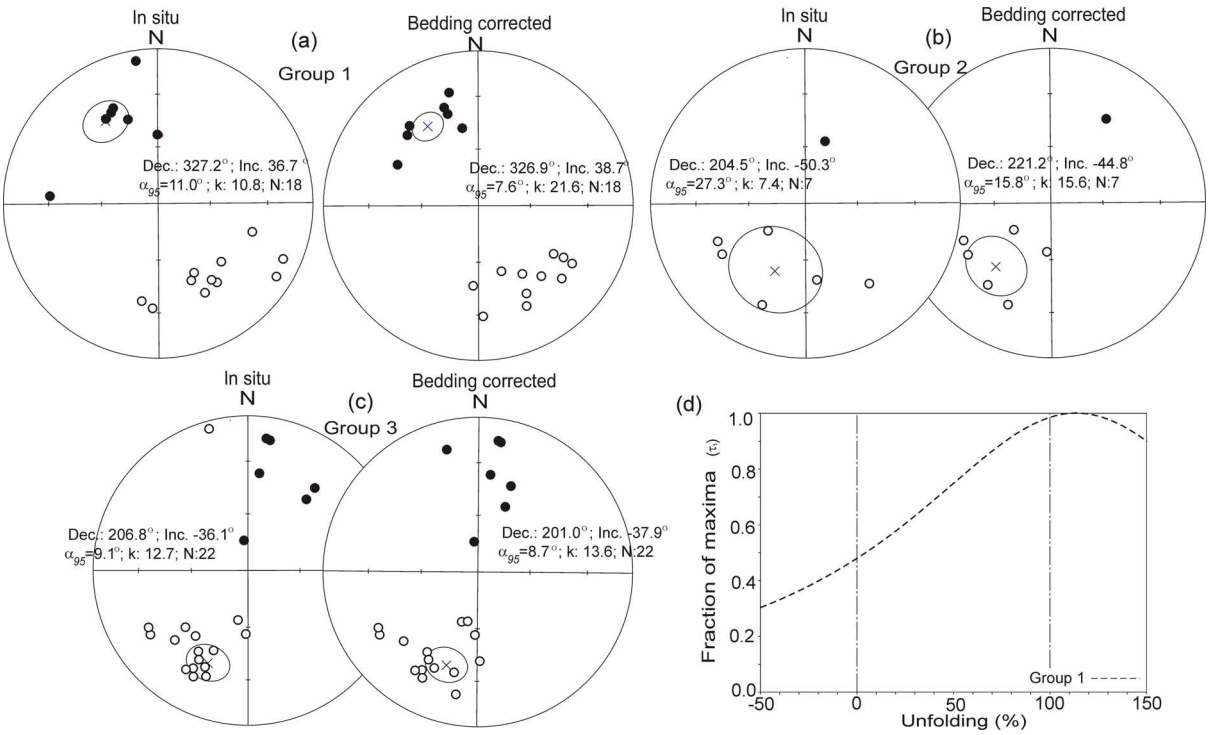

Figure 8. a-c) Equal-area stereographic projections showing the paleomagnetic site mean directions and 95 percent confidence limits for groups 1-3. Solid (open) symbols on lower (upper) hemisphere. d) McFadden [1990] fold test for Group 1 (Bergama).

6. Discussion

The three observed group mean directions are compared with directions calculated from Eurasian Global Apparent Wander Path reference poles after Torsvik et al. [2012] using R. Enkin's unpublished PMGSC [2004] software. The lower-middle Miocene volcanic rocks of Group 1, separated from Groups 2 and 3 by SE-NW and ENE-WSW trending faults to the west and south, respectively (i.e. the Altınova and Bergama Fault Zones), exhibit a distinct counterclockwise rotation of R ± ΔR = -38.1° ± 6.4°. A clockwise rotation of R ± ΔR = + 35.6° ± 13.2° is estimated from Group 2 data in the tectonic block defined by the Zeytindağ area. The Group 3 block in the Dikili area, separated from the Zeytindağ Block by a NE-SW striking fault, experienced modest clockwise rotation by R ± ΔR = + 12.5° ± 7.4°.

Uzel et al. [2015] inferred paleomagnetism-based rotations along a transfer zone, named the SSW-NNE trending İBTZ (Figure 1), and proposed a two-stage extension model. Clockwise rotation of 22 ± 11° in the lower Miocene and a counterclockwise rotation of 25 ± 14° in middle to late Miocene time along the transfer zone were attributed to an orthogonal deformation controlled by detachment and strike-slip faults.

Van Hinsbergen et al. [2010] reported a rotational difference between the northern and southern Menderes Massif of ~25° – 30°. The authors considered the different senses of vertical axis rotation to be compatible with extension related to exhumation of the Menderes Metamorphic Core Complex, which formed during back-arc extension in the eastern part of the Aegean region. Platzman et al. [1998] and Kissel et al. [2003], however, interpreted their results in terms of a rotation of the entire Anatolian plate in a counterclockwise sense by ~20° – 30° since the middle Miocene. In contrast, data from lower Miocene volcanic rocks from the Chios area by Kondopoulou et al. [2011] implied a chaotic rotation pattern, and Uzel et al. [2015] reported a poorly defined result from the Karaburun península with a large error envelope (−8 ± 30°). Westerweel et al. [2020] presented early Miocene paleomagnetic clockwise rotations of 29° ± 5° in the Soma Basin which they ascribed to the İBTZ as a dextral shear zone, whereas counterclockwise rotation of 21° ± 12° in the late Miocene was related to widespread extension as a result of the subduction of the African plate below the Aegean region.

Neogene tectonics of the Aegean region are characterized by continental collision between the Arabian and Eurasian Plates and westward escape of the Anatolian block along the North and East Anatolian fault zones [McKenzie, 1989; Barka and Reilinger, 1997]. The driving mechanism in upper-plate extension in the Aegean region has been assigned to NNE subduction of the African plate beneath the Aegean trench and slab rollback along the Hellenic trench since 30 Ma [Royden, 1993; Jolivet and Faccenna, 2000; Faccenna et al., 2003; van Hinsbergen et al., 2005].

Our new paleomagnetic results, based on a relatively limited dataset, reveal rotations of statistically significant opposite sense among three different small crustal blocks, suggesting crustal rotations on a rather local scale. Complex magmatic activity in Western Anatolia took place during two cycles, when lavas and pyroclastic products initially were emplaced during the early to middle Miocene (Figure 9a) and secondly shoshonitic volcanic rocks (basaltic to trachy-andesitic) were emplaced in the middle Miocene. In the Dikili and Zeytindağ blocks, clockwise rotations of about 12° and about 36° are obtained for this time period. Farther north, in the Bergama block, counterclockwise rotation of about 38° is observed (Figure 9b). We suggest that scissors-like opening of the Bakırçay graben is responsible for counterclockwise rotation of Block 1 (Bergama) and clockwise rotations of Blocks 2 and 3 (Zeytindağ, Dikili) (Figure 9 b, c). Each block was in the latest tectonic phases surrounded by dextral faults to the north and south lasting into the Quaternary. Sangu et al. [2020] recently named these structures as the right lateral Altınıova, Çandarlı, Bergama and Gülbahçe oblique faults (Figure 9c). Further displacement along these faults may have resulted in varying amounts of rotations which may escape paleomagnetic resolution.

On a larger scale, the pattern of differential block rotation could be accommodated by the N-S extension of the western Anatolian area, as several smaller fragmented crustal blocks were rotated with respect to one another to result in the present distribution of extensional basins. From the early to late Miocene, the overall region experienced about 45° of CW rotation, yet during the same time interval the Menderes part to the south experienced a compatible 48° CCW rotation [Van Hinsbergen et al., 2010; Uzel et al., 2015]. These large magnitudes of counterclockwise and clockwise rotations, however, could not only be explained by basin evolution over a small scale area. Therefore the counterclockwise rotation of Anatolia during its westwards escape must have also had a significant control in this rotational pattern. Uzel et al. [2015] suggested that the displacement along the İBTZ, which lies SE of the study area, should also affect areas that are outside this transfer zone. If this hypothesis is reasonable, it may explain why the Zeytindag block, which is situated immediately within the zone, experienced a greater amount of clockwise rotation, compared to the Dikili block. In addition, the contribution of the westward escape of the Anatolian block and the slab rollback along the Hellenic trench also needs to be considered, together with displacement along the NNE-SSW trending İBTZ during tectonic deformation. Therefore, the influence of smaller scale differential rotations resulting from relative displacement along grabens bounding faults should not be neglected when considering tectonic rotations in the context of the regional Aegean region deformation.

7. Conclusions

Paleomagnetic data from lower to middle Miocene volcanic rocks in the Dikili area and adjacent structural blocks provide evidence for the presence of three separate structurally detached crustal elements that are delineated from each other by NW-SE and E-W oriented normal faults. Group 1, which is defined as the Bergama Block, yields data suggesting counterclockwise rotation of $R \pm \Delta R = -38.1° \pm 11.1°$. On the other hand, clockwise rotations of $R \pm \Delta R = 35.6° \pm 13.2°$ and $R \pm \Delta R = 12.5° \pm 7.4°$ are obtained for Group 2, (Zeytindağ Block), and Group 3, (Dikili Block), which are separated by a ENE-WSW trending graben and fault system (cf. Bergama, resp. Zeytindağ graben in Figure 2).

Considering regional tectonics, our study is focused on an area of tectonic escape and subduction-related extension [e.g. McKenzie, 1970; Dewey and Şengör, 1979; Le Pichon and Angelier, 1979], that is locally delimited by NE–SW and NW–SE trending strike slip faults and E-W trending normal faults [Westerweel et al., 2020; Sangu et al., 2020]. Our paleomagnetic results provide evidence of relatively small, contiguous blocks, which show both clockwise and counterclockwise rotations of different magnitude. They were deformed from the early Miocene to the Present as a result of extension, scissor-like basin evolution and faulting in the eastern Aegean region, in connection with the westward escape of Anatolia.

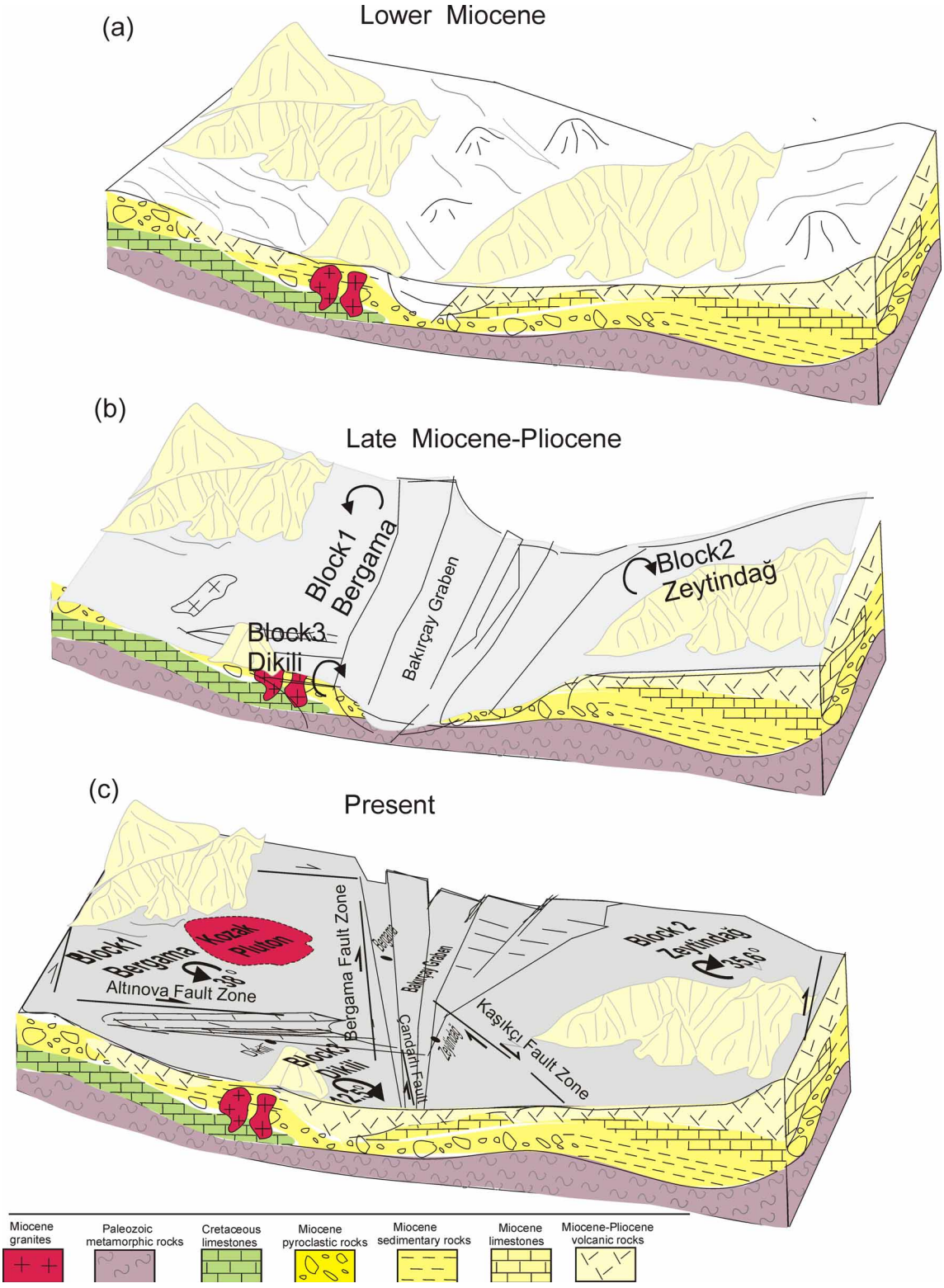

Figure 9. Kinematic evolution of the Dikili, Bergama and Zeytindağ microblocks in Western Anatolia showing tectonic rotations after the Lower Miocene. a) Evolution of Lower Miocene volcanic rocks experienced counterclockwise rotation during NE-SW extension and the westwards movement of Anatolia. b) After Pliocene, the formation of the Bakırçay graben seperated several crustal blocks named as Dikili, Zeytindağ and Bergama from each other. c) The influence of dextral faults in the north led to counterclockwise rotation of the Bergama block, while the evolution of the Bakırçay graben provoked clockwise rotation in the Dikili and Zeytindağ blocks.

Acknowledgements. The authors would like to thank the city manager and employees of the city of Dikili for their support in transportation and accommodation. Undergraduate students of the Istanbul University Department of Geophysical Engineering are very much appreciated for their assistance during field work. This study was supported by the Scientific Research Project Coordinatory of Istanbul University Project number: YADOP 49024. John Geissman is very much acknowledged for his kind remarks on this manuscript. The authors are greatful to John Geissman, Bora Uzel, John Piper and an anonymous reviewer for their valuable suggestions that improved the manuscript.

References

Akyürek, B. and Y. Soysal (1983). Biga yarımadası güneyinin (Savaştepe- Kırkağaç-Bergama-Ayvalık) temel jeoloji özellikleri, Bull. Min. Res. Exp., 95/96, 1-13.

Aldanmaz, E., J. Pearce, M.F. Thirlwall and J.G. Mitchell (2000). Petrogenetic evolution of Late Cenozoic, post-collision volcanism in western Anatolia, Turkey, J. Volcanol. Geoth. Res., 102, 1-2, 67-95.

Altıner, D. and T.A. Koçyiğit (1993). Third remark on the geology of Karakaya basin. An Anisian megablock in northern central Anatolia: micropaleontologic, stratigraphic and tectonic implications for the rifting stage of Karakaya basin, Turkey, Revue de Paléobiologie, 12, 1-17.

Altunkaynak, Ş. (1996). Geologic and petrologic investigation of the relationship of young volcanism and plutonism in the area Located between Bergama and Ayvalık, PhD Thesis, Technical University of İstanbul, Institute of Science, Turkey, 402 (Turkish with an extended English abstract).

Altunkaynak, Ş. and Y. Yılmaz (1998). The mount Kozak magmatic complex, western Anatolia, J. Volcanol. Geotherm. Res., 85, 1, 211-231.

Altunkaynak, Ş. and Y. Yılmaz (1999). The Kozak Pluton and its emplacement, Geol. J, 34, 3, 257-274.

Archanjo, C.J., R.I. Trindade, J.W.P. Macedo and G. Araujo (2000). Magnetic Fabric of a Basaltic Dyke Swarm Associated with Mesozoic Rifting in Northeast Brazilian, J. South Am. Earth. Sci., 13, 179-189.

Barka, A.A. and C.K. Kadinsky (1988). Strikeslip fault geometry in Turkey and its influence on earthquake activity, Tectonics, 7, 3, 663-684.

Barka, A. (1992). The north Anatolian fault zone, Ann. Tectonic., 6, 164-195.

Barka, A. and R. Reilinger (1997). Active tectonics of the Eastern Mediterranean region: deduced from GPS, neotectonic and seismicity data, Annali Geofisica., 40, 587-610.

Benda, L., F. Innocenti, R. Mazzuoli and S.P. Radicati (1974). Stratigraphic and radiometric data of the Neogene in Northwest Turkey, Z. Dtsch. Geol. Ges., 125, 183-193.

Bingöl, E., B. Akyürek and B. Korkmazer (1973). Geology of the Biga Peninsula and some characteristics of the Karakaya formation, Congr. on Earth Sci. for the 50th Ann. of Rep. of Turkey, Abstracts, 70-77 (in Turkish with English abstract).

Bingöl, E., M. Delaloye and G. Ataman (1982). Granitic intrusions in western Anatolia: a contribution to the geodynamic study of this area, Eclogae Geol. Helv., 75, 2, 437-446.

Borsi, S., G. Ferrara, F. Innocenti and R. Mazzuoli (1972). Geochronology and petrology of recent volcanics in the eastern Aegean sea (West Anatolia and Lesvos Island), Bull. Volcanol, 36, 473-496.

Bozkurt, E. (2000). Timing of extension on the Büyük Menderes Graben, western Turkey, and its tectonic implications, J. Geol. Soc. London., Spec. Publ., 173, 1, 385-403.

Bozkurt, E. (2003). Origin of NE-trending basins in western Turkey, Geodin. Acta, 16, 2-6, 61-81.

Bozkurt, E. and H. Sözbilir (2004). Tectonic evolution of the Gediz Graben: field evidence for an episodic, two-stage extension in western Turkey, Geol. Mag., 141, 1, 63-79.

Canon-Tapia. E., G.P.K. Walker and E. Herrero-Bervera (1996). The internal structure of lava flows – insights from AMS measurements, J. Volcanol. Geotherm. Res., 70, 21-36.

Cox, A. (1969). Geomagnetic reversals, Science, 163, 3864, 237-245.

Deenen, M.H.L., C.G. Langereis, D.J.J. Van Hinsbergen and A.J. Biggin (2011). Geomagnetic secular variation and the statistics of paleomagnetic directions, Geophys. J. Int., 186, 509-520.

Dewey, J.F. and A.M.C. Şengör (1979). Aegean and surrounding regions: complex multiplate and continuum tectonics in a convergent zone, Geol. Soc. Am. Bull., 90, 1, 84-92.

Dewey, J.F., M.R. Hempton, W.S.F. Kidd, F. Saroglu and A.M.C. Şengör (1986). Shortening of continental lithosphere:

The neotectonics of Eastern Anatolia–a young collision zone, In: MP Coward and AC Ries (eds), Collision Tectonics. J. Geol. Soc. London., Spec. Publ., 19, 3-36.

Dilek, Y. and Ş. Altunkaynak (2009). Geochemical and temporal evolution of Cenozoic magmatism in Western Turkey: Mantle response to collision, slab break-off, and lithospheric tearing in an orogenic belt. J. Geol. Soc. London., Spec. Publ., 311, 1, 213-233.

Doglioni, C., S. Agostin, M. Crespi, F. Innocenti, P.Manetti, F. Riguzzi and Y. Savascın (2002). On the extension in western Anatolia and the Aegean sea, J. Virtual Explor., 7, 117-131.

Ellwood, B.B. (1978). Flow and emplacement direction determined for selected basaltic bodies using magnetic susceptibility anisotropy measurements, Earth. Planet. Sci. Lett., 41, 254-264.

Emre, Ö., T.Y. Duman, Ş. Özalp, F. Şaroğlu, Ş. Olgun, H. Elmacı and T. Can (2018). Active fault database of Turkey. Bull. Earthq. Eng., 16, 8, 3229-3275.

Enkin, R.J., (2004). Paleomagnetism Data Analysis: Version 4.2. Geol. Surv. Can., Sidney, BC.

Ercan, T., M. Satır, H. Kreuzer, A. Türkecan, E. Günay, A. Çevikbaş, M. Ateş and B. Can (1985). Interpretation of chemical, isotopic and radiometric data of Western Anatolia Cenozoic volcanics, Geo. Bull. of Turkey, 28, 121-136 (in Turkish with English abstract).

Ersoy, Y.E., C. Helvacı and M.R. Palmer (2011). Stratigraphic, structural and geochemical features of the NE–SW trending Neogene volcano-sedimentary basins in western Anatolia: implications for associations of supra-detachment and transtensional strike-slip basin formation in extensional tectonic setting, J. Asian. Earth. Sci., 41, 2, 159-183.

Faccenna, C., L. Jolivet, C. Piromallo and A. Morelli (2003). Subduction and the depth of convection in the Mediterranean mantle, J. Geophys. Res. Solid. Earth., 108, B2, 2099.

Fisher, R.A. (1953). Dispersion on a sphere, Proc. R. Soc. Lond. A., 217, 1130, 295-305.

Genç, Ş.C. and Y. Yılmaz (1995). Evolution of the Triassic continental margin, northwest Anatolia, Tectonophysics, 243, 1-2, 193-207.

Genç, C.Ş., Ş. Altunkaynak, Z. Karacık, M. Yazman and Y. Yılmaz (2001). The Çubukludağ graben, south of İzmir: its tectonic significance in the Neogene geological evolution of the western Anatolia, Geodin. Acta, 14, 1-3, 45-55.

Geoffroy, L., J.P. Callot, C. Aubourg and M. Moreira (2002). Magnetic and plagioclase linear fabric discrepancy in dykes: a new way to define the flow vector using magnetic foliation, Terra Nova, 14, 183-190.

Gil, A., M. Lago, C. Gale, A. Pocovia and E. Arranz (2002). Magnetic fabric in folded sills and lava flows. A case study in the Permian basalts of the Anayet Massif (Pyrenean Axial Zone, Spain), Tectonophysics, 350, 1-15.

Görür, N., A.M.C. Sengör, M. Sakınç, R. Akkök, E. Yiğitbaş, F.Y. Oktay and Ş. Ersoy (1995). Rift formation in the Gökova region, southwest Anatolia: implications for the opening of the Aegean Sea. Geol. Mag., 132, 6, 637-650.

Güleç, N. (1991). Crust-mantle interaction in western Turkey: implications from Sr and Nd isotope geochemistry of Tertiary and Quaternary volcanics, Geol. Mag., 23, 417-435.

Gürsoy, H., O. Tatar, J.D.A. Piper, F. Koçbulut, Z. Akpınar, B. Huang, A.P. Roberts and B.L. Mesci (2011). Palaeomagnetic study of the Kepezdağ and Yamadağ volcanic complexes, central Turkey: Neogene tectonic escape and block definition in the central-east Anatolides, J. Geodyn., 51, 5, 308-326.

Herrero-Bervera, E., G.P.L. Walker, E. Canon-Tapia and M.O. Garcia (2001). Magnetic fabric and inferred flow direction of dikes, conesheets and sill swarms, Isle of Skye, Scotland, J. Volcanol. Geotherm. Res., 106, 195-210.

Hou, Z., Z. Yang, Y. Lu, A. Kemp, Y. Zheng, Q. Li and L. Duan (2015). A genetic linkage between subduction- and collision-related porphyry Cu deposits in continental collision zones, Geology, 43, 3, 247-250.

Huguen, C., J. Mascl, E. Chaumillon, J.M. Woodside, J. Benkheli, A. Kopf and A.Volkonskaïa (2001). Deformational styles of the eastern Mediterranean Ridge and surroundings from combined swath mapping and seismic reflection profiling, Tectonophysics, 343, 1-2, 21-47.

Işık, V. and O. Tekeli (2001). Late orogenic crustal extension in the northern Menderes massif (western Turkey): evidence for metamorphic core complex formation, Int. J. Earth. Sci., 89, 4, 757-765.

İşveren, T., M.C. Tapırdamaz, F. Özçep, M. Hisarlı, N. Orbay and M. Sanver (1995). "Kuzeybatı Anadolu'nun tektoniği ve paleomanyetik sonuçlar", Jeofizik Dergisi 9.

Jelínek, V. (1977). The statistical theory of measuring anisotropy of magnetic susceptibility of rocks and its application, Brno. Geofyzika, 1-88.

Jelínek, V. (1978). Statistical processing of magnetic susceptibility measured in groups of specimens, Studia. Geophys.

et Geod., 22, 50-62.
Jelínek, V. (1981). Characterization of the magnetic fabric of rocks. Tectonophysics, 79:63-67.
Jolivet, L. and C. Faccenna (2000). Mediterranean extension and the Africa-Eurasia collision, Tectonics, 19, 6, 1095-1106.
Karacık, Z. and Y. Yılmaz (1998). Geology of the ignimbrites and the associated volcano–plutonic complex of the Ezine area, northwestern Anatolia, J. Volcanol. Geotherm. Res., 85, 1, 251-264.
Karacık, Z., Y. Yılmaz and J.A. Pearce (2007). The Dikili-Çandarlı volcanics, Western Turkey: magmatic interactions as recorded by petrographic and geochemical features, Turkish J. Earth Sci., 16, 4, 493-522.
Kaymakçı, N., E. Aldanamaz, C. Langereis, T.L. Spell, O.F. Gürer and K.A. Zanetti (2007). Late Miocene transcurrent tectonics in NW Turkey: evidence from paleomagnetic and ^{40}Ar-^{39}Ar dating of alkaline volcanic rocks, Geol. Mag., 144, 2, 699-718.
Kirschvink, J.L. (1980). The least squares line and plane and the analysis of paleomagnetic data, Geophys. J. R. Astron. Soc., 62, 699-718.
Kissel, C., C. Laj, A Poisson and N. Görür (2003). Paleomagnetic reconstruction of the Cenozoic evolution of the eastern Mediterranean, Tectonophysics, 362. 199–217, doi:10.1016/S0040-1951(02)00638-8.
Knight, M.D. and G.P.L. Walker (1988). Magma flow directions in dikes of the Koolau Complex, Oahu, determined from magnetic fabric studies, J. Geophys. Res., 93, 4301-4319.
Koçyiğit, A. (1987). Hasanoglan (Ankara) yoresinin tektono-stratigrafisi: Karakaya orojenik kusaginin evrimi (Tectono-stratigraphy of the Hasanoglan region: Evolution of the Karakaya Orogeny). Hacettepe University Earth Sciences, Special Publication, 14, 269-293.
Koçyiğit, A., H. Yusufoğlu and E. Bozkurt (1999). Evidence from the Gediz graben for episodic two-stage extension in western Turkey, Geol. Soc. Lond. London, 156, 605-616.
Kondopoulou, D., S. Sen, E. Aidona, D.J.J. Van Hinsbergen and G. Koufos (2011). Rotation history of Chios island, Greece since the Middle Miocene. J. Geodyn., 51(5):327-338.
Kurt, H., Demirbağ, E. and İ. Kuşçu (1999). Investigation of the submarine active tectonism in the Gulf of Gökova, southwest Anatolia–southeast Aegean Sea, by multi-channel seismic reflection data, Tectonophysics, 305, 4, 477-496.
Lauer, J.P. (1984). Geodynamic evolution of Turkey and Cyprud based on paleomagnetic data, J. Geol. Soc. London., Spec Pub., 17, 1, 483-491.
Le Pichon, X. and J. Angelier (1979). The Hellenic Arc and Trench System: A Key to the Neotectonic Evulotion of the Eastern Mediternean Area, Tectonophysics, 60, 1979, 1-42.
Le Pichon, X. and J. Angelier (1981). The Aegean Sea, Philos. Trans. R. Soc. Lond. A, 300, 1454, 357-372.
Lips, A.L., D. Cassard, H. Sözbilir, H. Yılmaz and J.R. Wijbrans (2001). Multistage exhumation of the Menderes massif, western Anatolia (Turkey), Int.J. Earth. Sci., 89, 4, 781-792.
Loock, S., H. Diot, B. Van Wyk de Vries, P. Launeau, O. Merle, F. Vadeboin and M.S. Petronis (2008). Lava flow internal structure found from AMS and textural data: An example in methodology from the Chaîne des Puys, France, J. Volcanol. Geotherm. Res., 177, 1092-1104.
Lowrie, W. (1990). Identification of ferromagnetic minerals in a rock by coercivity and unblocking temperature properties, Geophys. Res. Lett., 17, 159-162.
McClusky. S., S. Balassanian, A. Barka, C. Demir, S. Ergintav, I. Georgiev, O. Gürkan, M. Hamburger, K. Hurst, H. Kahle, K. Kastens, G. Kekelidze, R. King, V. Kotzev, O. Lenk, S. Mahmoud, A. Mishin, M. Nadariya, A. Ouzounis, D. Paradissis, Y. Peter, M. Prilepin, R. Reilinger, I. Şanlı, H. Seeger, A. Tealeb, N. Toksöz and Veis G (2000). Global Positioning System constraints on plate kinematics and deformation in the eastern Mediterranean and Caucasus, J. Geophys. Res., 105, 5695-5719.
McClusky. S., R. Reilinger, S. Mahmoud, D. Ben Sari and A. Tealeb (2003). GPS constraints on Africa (Nubia) and Arabia plate motion, Geophys. J. Int., 155, 126-138.
McElhinny, M.W. (1964). Statistical significance of the fold test in palaeomagnetism, Geophys. J. R. Astron. Soc., 135, 338-340.
McElhinny, M.W. and P.L. McFadden (1997). Palaeosecular variation over the past 5 Myr based on a new generalized database, Geophys. J. Int., 131, 2, 240-252.
McFadden, P.L. and M.W. McElhinny (1990). Classification of the reversal test in palaeomagnetism, Geophys. J. Int., 103, 725-729.

McFadden, P.L. (1990). A new fold test for paleomagnetic studies, Geophys. J. Int., 103, 163-169.

McKenzie, D. (1970). Plate tectonics of the Mediterranean region, Nature, 226, 5242, 239-243.

McKenzie, D. (1978). Some remarks on the development of sedimentary basins, Earth Planet. Sci. Lett., 40, 25-32.

McKenzie, D. (1989). Some remarks on the movement of small melt fractions in the mantle, Earth Planet. Sci. Lett., 95, 1-2 53-72.

Meulenkamp. J.E., G.J. Van Der Zwaan and W.A. Van Wamel (1994). On Late Miocene to Recent vertical motions in the Cretan segments of the Helennic Arc, Tectonophysics, 234, 53-72.

MTA (2002). Geological map series of Turkey, 1: 500 000 scale, 18 sheets: Maden Tetkik ve Arama Genel Müdürlüğü, Ankara.

Nebert, K. (1978). Das braunkohlenführende Neogengebiet von Soma, Westanatolien, Bull.Min.Res.Exp., 90, 20–72.

Okay, A. I. and M. Satır (2000). Coeval plutonism and metamorphism in a latest Oligocene metamorphic core complex in northwest Turkey, Geol. Mag., 137, 5, 495-516.

Orbay, M.N., M. Sanver, F. Özçep, T. İşseven and Z.M. Hisarlı and C. Tapırdamaz (2001). Bati Anadolu'nun Paleomağnetizmasi ve Jeodinamik Gelişimi. Jeofizik, cilt.15, 125-142.

Orbay, M.N., M. Sanver, C. Tapırdamaz, F. Özçep, T. İşseven and Z.M. Hisarlı (1998). The Paleomagnetism of South Thrace and North Biga Peninsula. Istanbul Univ. Müh. Fak. Yerbilimleri Dergisi, 11, 113-124 (in Turkish with English abstract).

Piper J.D.A., J.M. Moore, O. Tatar, H. Gursoy and R.G. Park (1996). Palaeomagnetic study of crustal deformation across an intracontinental transform: the North Anatolian Fault Zone in Northern Turkey, J. Geol. Soc. London., Spec. Publ., 105, 1, 299-310.

Piper, J.D.A, O. Tatar and H. Gürsoy (1997). Deformational behaviour of continental lithosphere deduced from block rotations across the North Anatolian fault zone in Turkey, Earth. Planet. Sci. Lett., 150, 3-4, 191-203.

Piper, D.J.W and C. Perissoratis (2003). Quaternary neotectonics of the South Aegean arc. Mar, Geol., 198, 3-4, 259-288.

Piper, J.D.A, H. Gürsoy, O. Tatar, M.E. Beck, A. Rao, F. Kocbulut and B.L. Mesci (2010). Distributed neotectonic deformation in the Anatolides of Turkey: a palaeomagnetic analysis, Tectonophysics, 488, 1-4, 31-50.

Platzman, E.S., C. Tapirdamaz and M. Sanver (1998). Neogene anticlockwise rotation of central Anatolia (Turkey): preliminary paleomagnetic and geochronological results, Tectonophysics, 299, 1-3, 175-189.

Royden, L.H. (1993). The tectonic expression slab pull at continental convergent boundaries, Tectonics, 12, 2, 303-325.

Sangu, E., Ö.F. Gürer and A. Gürer (2020). Fault kinematic and Plio-Quaternary paleostress evolution of the Bakırcay Basin, Western Turkey. Int. Geol. Rev., 62, 10, 1245-1261.

Seyitoğlu, G. and B.C. Scott (1992). The age of the Büyük Menderes graben (west Turkey) and its tectonic implications, Geol. Mag., 129, 2, 239-242.

Seyitoğlu, G., N. Kazancı, K. Karakuş, L. Fodor, H. Araz and L. Karadenizli (1997). Does continuous compressive tectonic regime exist during Late Palaeogene to Late Neogene in NW Central Anatolia, Turkey? Preliminary observations, Turkish J. Earth Sci., 6, 77-83.

Sözbilir, H. (2001). Extensional tectonics and the geometry of related macroscopic structures: field evidence from the Gediz detachment, western Turkey, Turkish J. Earth Sci., 10, 2, 51-67.

Sözbilir, H. (2002). Geometry and origin of folding in the Neogene sediments of the Gediz Graben, western Anatolia, Turkey, Acta Geod, 15, 5-6, 277-288.

Sözbilir, H. and T. Emre (1996). Supradetachment basin and rift basin developed during the neotectonic evolution of the Menderes Massif, In: Geol. Soc. of Turkey, Ankara, Abstracts 300-301.

Şengör, A.M.C. (1979). Tethys and its implications, Nature, 279, 14, 14.

Şengör, A.M.C. (1980). Principles of the neotectonics of Turkey, In: Geol. Soc. of Turkey, Conference Series 2.

Şengör, A.M.C., N. Görür and F. Şaroğlu (1985). Strike-slip faulting and related basin formation in zones of tectonic escape: Turkey as a case study. In: Biddle, K.T. and Christie- Blick, N. (Eds), Strike-slip Deformation, Basin Formation and Sedimentation, Soc. of Econ. Min. and Paleo. Spec. Pub., 37, 227-264.

Stampfli, G.M. (2000). Tethyan ocean. In: E Bozkurt, JA Winchester, JDA Piper (eds.), Tectonics and magmatism in Turkey and surrounding area, J. Geol. Soc. London., Spec. Publ., 173, 1-23.

Tatar, O., Z. Akpınar, H. Gürsoy, J.D.A. Piper, F. Koçbulut, B.L. Mesci, A. Polat and A.P. Roberts (2013). Palaeomagnetic evidence for the neotectonic evolution of the Erzincan Basin, North Anatolian Fault Zone, Turkey. J. Geodyn, 65, 244-258.

Tauxe, L. (1998). Paleomagnetic Principles and Practice. Kluwer Academic Publishers, Dordrecht, 312.

Taymaz, T. (1990). Earthquake source para.meters in the Eastern Mediterranean Region, PhD Thesis, Darwin College, University of Cambridge, U.K, 244.

Taymaz, T., Jackson J, McKenzie D (1991). Active tectonics of the north and central Aegean Sea, Geophys. J. Int., 106, 2, 433-490.

Taymaz, T., Yılmaz Y, Dilek Y (2007). The geodynamics of the Aegean and Anatolia: Introduction, J. Geol. Soc. London., Spec. Publ., 291, 1, 1-16.

Torsvik, T.H., R. Van der Voo, U. Preeden, C. Mac Niocaill, B. Steinberger, P.V. Doubrovine and J.G. Meert (2012). Phanerozoic polar wander, palaeogeography and dynamics, Earth. Sci. Rev., 114, 3-4, 325-368.

Uzel, B., C.G. Langereis, N. Kaymakçı, H. Sözbilir, Ç. Özkaymak, M. Özkaptan (2015). Paleomagnetic evidence for an inverse rotation history of Western Anatolia during the exhumation of Menderes core complex. Earth Planet. Sci. Lett., 414, 108–125.

Uzel, B., Ö. Sümer, M. Özkaptan, Ç. Özkaymak, K. Kuiper, H. Sözbilir, N. Kaymakçi, U. İnci, C.G. Langereis (2017). Palaeomagnetic and geochronological evidence for a major middle Miocene unconformity in Söke Basin (western Anatolia) and its tectonic implications for the Aegean region, J. Geol. Soc. London., 174, 4, 721-740.

Uzel, B., K. Kuiper, H. Sözbilir, N. Kaymakci, C.G. Langereis and K. Boehm (2020). Miocene geochronology and stratigraphy of western Anatolia: Insights from new Ar/Ar dataset, Lithos, 352, 105-305.

Van Hinsbergen, D.J.J., E. Hafkenscheid, W Spakman, J.E. Meulenkamp and R. Worte (2005). Nappe stacking resulting from subduction of oceanic and continental lithosphere below Greece, Geology, 33, 4, 325-328.

Van Hinsbergen, D.J.J. (2010). A key extensional metamorphic complex reviewed and restored: the Menderes Massif of western Turkey, Earth. Sci. Rev., 102, 1-2, 60-76.

Van Hinsbergen, D.J.J., N. Kaymakçı, W. Spakman and T.H. Torsvik (2010). Reconciling the geological history of western Turkey with plate circuits and mantle tomography, Earth. Planet. Sci. Lett., 297, 3-4, 674-686.

Westaway, R. (1994). Present day kinematics of the Middle East and eastern Mediterranean, J. Geophys. Res. Solid Earth., 99, B6, 12071-12090.

Westerweel, J., B. Uzel, C.G. Langereis, N. Kaymakçi amd H. Sözbilir (2020). Paleomagnetism of the Miocene Soma basin and its structural implications on the central sector of a crustal-scale transfer zone in western Anatolia (Turkey), J. Asian Earth Sci., 193, 104305.

Woodside, J., J. Mascle, C. Huguen and A. Volkonskaia (2000). The Rhodes Basin, a post-Miocene tectonic trough, Mar. Geol., 165, 1-4, 1-12.

Yılmaz, Y, (1989). An approach to the origin of young volcanic rocks of western Turkey, In: Şengor, A.M.C. (Ed), Tectonic Evolution of the Tethyan Region. Kluwer Academic Publication, The Hague, 159-189.

Yılmaz, Y., Ş.C. Genç, F. Gürer, M. Bozcu, K. Yılmaz, Z. Karacık,Ş. Altunkaynak and A. Elmas (2000). When did the western Anatolian grabens begin to develop? In: E. Bozkurt, J.A. Winchester and J.D.A. Piper (Eds), Tectonics and Magmatism in Turkey and the Surrounding Area, J. Geol. Soc. London., Spec. Publ., 173, 353-384.

Yılmaz, Y. (2017). Morphotectonic development of Anatolia and the surrounding regions. In: Çemen İ, Yılmaz Y (eds), Active Global Seismology: Neotectonics and Earthquake Potential of the Eastern Mediterranean Region, Geophys. Monogr. Ser., Am. Geoph. Uni., John Wiley & Sons, New York, 225, 11-91.

Zijderveld, J.D.A. (1967). AC demagnetization of rocks: analysis of results, in: DW Collinson, KM Creer and SK Runcorn (Eds), Methods in Palaeomagnetism. Elsevier, Amsterdam, 245-286.

***CORRESPONDING AUTHOR: Mualla CENGIZ**,
Istanbul University-Cerrahpaşa, Faculty of Engineering, Department of Geophysical Engineering,
34800 Hadımköy, İstanbul, Turkey,
e-mail address: mualla@iuc.edu.tr